HHS Public Access

Author manuscript

Anal Chem. Author manuscript; available in PMC 2022 June 22.

Published in final edited form as:

Anal Chem. 2021 June 22; 93(24): 8476–8483. doi:10.1021/acs.analchem.1c00716.

Low-cost High-Pressure Clinical-Scale 50% Parahydrogen Generator Using Liquid Nitrogen at 77 K

Benjamin Chapman[b], **Baptiste Joalland**[c], **Collier Meersman**[a], **Jessica Ettedgui**[d], **Rolf E. Swenson**[d], **Murali C. Krishna**[e], **Panayiotis Nikolaou**[f], **Kirill V. Kovtunov**[g,h], **Oleg G. Salnikov**[g,h,i], **Igor V. Koptyug**[g], **Max E. Gemeinhardt**[j], **Boyd M. Goodson**[j,k], **Roman V. Shchepin**[a], **Eduard Y. Chekmenev**[c,l,*]

[a]Department of Chemistry, Biology, and Health Sciences, South Dakota School of Mines and Technology, 501 E St. Joseph Street Rapid City, South Dakota 57701, United States

[b]Department of Materials and Metallurgical Engineering, South Dakota School of Mines and Technology, 501 E St. Joseph Street Rapid City, South Dakota 57701, United States

[c]Department of Chemistry, Integrative Biosciences (Ibio), Wayne State University, Karmanos Cancer Institute (KCI), 5101 Cass Ave, Detroit, Michigan 48202, United States

[d]Chemistry and Synthesis Center, National Heart, Lung, and Blood Institute, 9800 Medical Center Drive, Building B, Room #2034, Bethesda, Maryland 20850, United States

[e]Center for Cancer Research, National Cancer Institute, National Institutes of Health, Bethesda, 31 Center Drive Maryland 20814, United States

[f]XeUS Technologies LTD, Georgiou Karaiskaki 2A, Lakatamia 2312, Nicosia, Cyprus

[g]International Tomography Center, SB RAS, 3A Institutskaya St., Novosibirsk 630090, Russia

[h]Novosibirsk State University, 2 Pirogova St., Novosibirsk 630090, Russia

[i]Boreskov Institute of Catalysis SB RAS, 5 Acad. Lavrentiev Pr., Novosibirsk, 630090, Russia

[j]Department of Chemistry and Biochemistry, Southern Illinois University, 1245 Lincoln Drive, Carbondale, Illinois 62901, United States

[k]Materials Technology Center, Southern Illinois University, 1245 Lincoln Drive, Carbondale, Illinois 62901, United States

[l]Russian Academy of Sciences, Leninskiy Prospekt 14, Moscow, 119991, Russia

Abstract

We report on a robust and low-cost parahydrogen generator design employing liquid nitrogen as coolant. The core of the generator consists of catalyst-filled spiral copper tubing, which can be pressurized to 35 atm. Parahydrogen fraction >48% was obtained at 77 K with three nearly identical generators using paramagnetic hydrated iron oxide catalyst. Parahydrogen quantification was performed on the fly via bench-top NMR spectroscopy to monitor the signal from residual

[*]**Corresponding Author**: chekmenevlab@gmail.com.

EYC, PN, and BMG declare a stake of ownership in XeUS Technologies, LTD.

orthohydrogen—parahydrogen is NMR silent. This real-time quantification approach was also used to evaluate catalyst activation at up to 1.0 standard liter per minute flow rate. The reported inexpensive device can be employed for a wide range of studies employing parahydrogen as a source of nuclear spin hyperpolarization. To this end, we demonstrate the utility of this parahydrogen generator for hyperpolarization of concentrated sodium [1-^{13}C]pyruvate, a metabolic contrast agent under investigation in numerous clinical trials. The reported pilot optimization of SABRE-SHEATH hyperpolarization yielded ^{13}C signal enhancement of over 14,000-fold at clinical relevant magnetic field of 1 T corresponding to approximately 1.2% ^{13}C polarization – if near 100% parahydrogen would have been employed, the reported value would be tripled to ^{13}C polarization of 3.5%.

Graphical Abstract

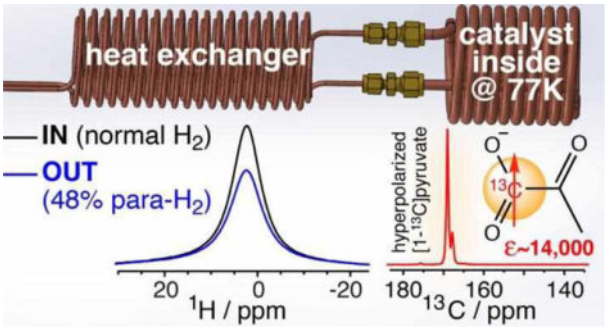

INTRODUCTION

NMR hyperpolarization techniques enhance the detection sensitivity of NMR spectroscopy and imaging by several orders of magnitude.[1–4] These tremendous gains in detection sensitivity enable new applications, including molecular imaging of exogenous contrast agents.[5–7] The nuclear spins of these new contrast agents are hyperpolarized (HP) using a wide range of techniques.[1, 8–10] Some hyperpolarization techniques have been successfully employed in clinical trials.[11–14] Despite the major successes in clinical research, none of these methods have enjoyed widespread or routine clinical use so far, in part because of high instrumentation cost and low hyperpolarization throughput.[14]

Parahydrogen-Induced Polarization (PHIP) is a simple, fast, and low-cost hyperpolarization approach[15–16] that has the potential to revolutionize production of HP contrast agents for clinical use. Canonical PHIP requires pairwise parahydrogen (p-H_2) addition to an unsaturated molecular substrate.[17–18] More recently, the non-hydrogenative variant called Signal Amplification by Reversible Exchange (SABRE) has emerged[19–20]: The latter method employs chemical exchange of p-H_2 and to-be-hyperpolarized substrates on metal complexes.[21–22] Both PHIP and SABRE approaches have produced a range of HP contrast agents with some validation success in cellular and pre-clinical models[23–29] as also described in recent reviews.[10, 30–31]

Parahydrogen, employed as the source of nuclear spin order in PHIP,[15, 32–33] is produced by transient exposure of normal dihydrogen gas (with its ambient 1:3 para-to-ortho-state

distribution) to a low-temperature.[26, 34–38] Because p-H_2 is a lower energy state, the equilibrium shifts to the para- state at sufficiently low temperatures[39]; nearly 100% p-H_2 can be obtained at ≤20 K.[2, 40] When pure p-H_2 is employed for PHIP, near-unity proton polarization can be unlocked after the magnetic equivalence of the nascent p-H_2-derived protons is broken.[15, 17, 41] Moreover, in both hydrogenative PHIP and its non-hydrogenative variant SABRE, it has been demonstrated that the polarization of nascent p-H_2-devrived protons can be transferred via the network of spin-spin couplings to other spin-1/2 nuclei including ^{13}C,[24, 42–45] ^{15}N,[46–48] ^{1}H,[21] ^{31}P,[49] ^{19}F,[50–51] and others.[52] Nuclear spin polarization (P) values in excess of 50% have been demonstrated[53–55] when polarization transfer is optimized using pure p-H_2 gas.

Once one has a supply of p-H_2 in hand, the remaining hardware required to accomplish polarization transfer in PHIP and SABRE is relatively straightforward and low-cost (*e.g.*, approximately $10k for a setup employing a mass-flow controller and mu-metal shields for SABRE[56] or PHIP field cycling studies[57] at micro-tesla fields), because no cryogenic or high-field hardware is required. However, the ostensible need for pure p-H_2 would require the use of cryogenic equipment in the range of $50,000–125,000 (*e.g.*, Bruker or ARS generators),[26, 29, 34, 36, 58] representing a substantial investment and a barrier for those working in (or desiring to enter) the field of p-H_2-based hyperpolarization. Moreover, the quantification of the p-H_2 fraction is often required to ensure reproducible results in PHIP and SABRE. In the NMR hyperpolarization community, the measurement is typically performed using high-field NMR spectroscopic quantification of the residual orthohydrogen fraction—because p-H_2 is NMR silent[59]—although other methods have been demonstrated.[60–62] Once created, the p-H_2 gas can then be stored in pressurized aluminum cylinders for weeks.[34, 36, 63] The requirement of a high-field NMR spectrometer adds additional complexity and cost to the infrastructure for robust and reproducible operation of a p-H_2-based hyperpolarization facility. As an alternative, we have recently demonstrated that the residual orthohydrogen fraction in near-100% p-H_2 gas can be monitored in real time using low-field bench-top NMR spectroscopy.[64] Bench-top NMR spectrometers have substantially lower cost than high-field NMR devices; they are also portable, have a small footprint, require no cryogens to operate, and are increasingly becoming a standard “workhorse” in routine hyperpolarization studies.[65–67]

To mitigate the cost and complexity of cryogenic hardware, p-H_2 production can be conducted at liquid N_2 temperature (*ca.* 77 K at 1 atm) resulting in approximately 50% p-H_2 fraction.[38] Moreover, liquid He can also be employed as a chilling source resulting in 97.5% p-H_2 fraction.[63] The key disadvantage of using 50% (versus near 100%) p-H_2 is the reduction of the resulting hyperpolarization effect by a factor of ~3. Such substantial polarization decrease can be unforgiving for many signal-to-noise ratio (SNR)-challenged applications, *e.g.*, most notably *in vivo* studies.[27, 68] However, many other applications—including the development phase of PHIP and SABRE-based contrast agents—can be accomplished with this ‘lower’ p-H_2 grade, which is much easier and cheaper to achieve in practice.[69–71]

Several parahydrogen converter/generator designs employing a wide range of ortho-to-para conversion catalysts have been reported for operation at liquid N_2 temperature.[38, 62, 71–73]

Moreover, very recently liquid-He-based system has been employed in the production of nearly pure p-H_2 using an inexpensive design ($1,200 in parts),[63] although the design relies on liquid He (which may impose a substantial additional running cost and infrastructure), requires a ~90-min. cool-down time, and has limited production capacity at maximum specs (200 standard cubic centimeters per minute, sccm).

Here, we report a robust and inexpensive design of a p-H_2 generator for operation with liquid N_2 at a tested pressure of up to 35 atm. The reported design is based on more than ten years of experience in our laboratories. The produced compressed H_2 gas is quantified by 'real-time' NMR spectroscopy of exiting p-H_2 using a bench-top 1.4 T NMR spectrometer. The design reproducibility has been evaluated with 3 separately constructed devices. Moreover, we have also investigated ortho-para catalyst activation by catalyst exposure to >100 °C to achieve a production rate of 1,000 sccm with ~49% p-H_2 fraction. The utility of the reported device has been tested in the feasibility demonstration of [1-^{13}C]pyruvate hyperpolarization via SABRE, following the work of Duckett and co-workers.[74] HP [1-^{13}C]pyruvate is a leading HP contrast agent employed for tracking of metabolism *in vivo*[7, 11–12, 14] and is currently being evaluated in many clinical trials and preclinical models of numerous human diseases.[13–14, 75] Taken together, the reported design augmented by real-time p-H_2 quantification using benchtop NMR spectroscopy will hopefully be of interest not only to those already working in the field of NMR hyperpolarization in general (and p-H_2-based hyperpolarization in particular), but also to those seeking a low-barrier entryway into NMR hyperpolarization techniques.

MATERIALS AND METHODS

Generator design.

The core component employs copper tubing (0.25 in. outer diameter, OD; 0.03 in. wall; 0.19 in. inner diameter, ID, McMasterCarr, P/N 5174K21; ~115 cm length) that was filled with ~21 g of hydrated iron(III) oxide ($Fe_2O_3 \cdot H_2O$, 371254, Sigma-Aldrich, St. Louis, MO)—this material is produced as Ionex Type OP Catalyst (https://www.molecularproducts.com/products/ionex-type-op-catalyst Molecular Products, Louisville, Colorado, USA). Prior to loading, the catalyst material was purged of microparticles by mechanical filtration via ABN strainer cone funnels with disposable 190-micron mesh https://www.amazon.com/gp/product/B01H7PEHEK/. Each funnel was filled to ~1/5 of its capacity and the catalyst was washed with ethanol or isopropanol until washing liquid passing through it became practically colorless. The alcohol-washed catalyst was further washed by hexane until the washing liquid became colorless as well. The washed catalyst was placed in a glass beaker and dried overnight in the oven at ~60 ℃. If not removed, microparticles can degrade p-H_2 generator performance if they escape downstream of the cryogenic region. The catalyst-filled copper tube was wound into a spiral with ~2.36 in. (6 cm) OD consisting of approximately 6 turns [~2.75 in. (7 cm) height], Figure 1. The ends of the copper tubing were filled with glass wool to ensure the catalyst stays in the 0.25 in. copper tubing segment. Next, each end of the catalyst-filled 0.25 in. spiral tubing segment was adapted to a heat-exchange 0.125 in. OD copper tubing spiral (0.03 in. wall; 0.065 in. OD, McMasterCarr, P/N 5174K1;) using brass Yor-lok reducers (McMasterCarr, P/N 5272K214). The two

hollow spirals (~20 turns of similar diameter) made of 0.125 in. copper tubing are designed to serve two purposes. The 0.125 in. copper tubing spiral is reinforced by aluminum brackets (Figure 1) to enhance structural rigidity. In case of the liquid N_2 level is above these heat exchangers, the inlet heat exchanger allows for pre-cooling of the incoming H_2 gas. Alternatively, if the liquid N_2 level is below the heat exchangers, heat exchange between incoming and exiting hydrogen gas flows allows pre-cooling of the incoming H_2 gas while warming the exiting para-enriched H_2, Figure 1.

Experimental setup for 'real-time' bench-top NMR spectroscopy of hydrogen gas.

To monitor the p-H_2 enrichment on the fly, we have employed the setup described previously,[64] which was adapted for operation with the present generator, Figure 2. A high-pressure tank equipped with a dual-stage pressure regulator and containing ultra-high purity (>99.999%) hydrogen was connected to the input port of the generator using a Yor-lok brass coupling. The other end of the generator was connected directly to the input of a mass-flow controller (MFC; Sierra Instruments Inc., Monterey, California, USA, P/N C100L-DD-1-OV1-SV1-PV2-V1-S0, 1000 sccm model). The hydrogen tank pressure was set to ~125 PSI. The flexible 0.125 in. copper lines allow for easy maneuvering of the generator core to insert into/remove from the liquid N_2 bath (in a Styrofoam container) or exposing the catalyst-filled section to a heat gun for catalyst activation studies (see below). Parahydrogen quantification was performed using a 1.4 T NMR spectrometer operating at 61 MHz proton resonance frequency with gas samples at 8 atm (100 PSI overpressure) employing the following acquisition parameters: 1024 scans, 5 kHz spectral width, 52 ms acquisition time, 0.1 s repetition time, ~102 s total acquisition time, 90° excitation pulse of ~10 μs duration.

Parahydrogen quantification

Parahydrogen quantification was performed using the previously described method,[64] which was adapted for operation with the described generator. Briefly, on the day of the operation, the setup (Figure 2) was first operated at room temperature, *i.e.*, without a liquid N_2 bath. The MFC flow rate was set to 150 sccm, and the safety valve was set to 100 PSI overpressure (as confirmed by the pressure gauge, Figure 2). The valve was placed in the "OFF" position, and normal hydrogen was allowed to pass through the catheter and run through a standard 5 mm NMR tube equipped with a "Y" connector for 10 minutes. This "purge" stage was required to remove any residual air and moisture from the setup, and to fill the NMR tube to 100 PSI overpressure with normal H_2 gas (containing 75% o-H_2).

Next, the valve is switched to the "ON" position and the gas flow is directed via bypass rather than through the NMR tube. As a result, normal hydrogen (25% para-H_2 and 75% ortho-H_2) in the tube was not flowing during NMR acquisition (instead, the flow was directed via bypass). Next, an NMR spectrum of normal H_2 gas was acquired using the acquisition parameters listed above. The signal (integrated area under the curve, AUC) was computed using SpinSolveExpert software supplied by the vendor (Magritek, New Zealand). The corresponding signal from an empty NMR tube was also acquired and subtracted from each NMR measurement to account for any background signal using the same spectral processing parameters.

The generator's catalyst-filled spiral was then submerged into a liquid N_2 bath and allowed to equilibrate at cryogenic temperature for 10 min. with a continuous H_2 flow at 150 sccm. The valve was switched to the "OFF" position to direct the gas flow through the NMR tube for ~2 min. Next, the valve is switched "ON". As a result, the para-enriched hydrogen in the tube was not flowing during NMR acquisition (instead, the flow was directed via bypass). Next, an NMR spectrum of para-enriched H_2 gas was acquired using the acquisition parameters listed in the Figure 3 caption. The NMR signal was processed in the same fashion as for normal H_2 as described above. All measurements for p-H_2-enriched and normal H_2 gas were repeated three times and averaged. The p-H_2 fraction (f) was computed using Eq. 1:

$$f = 1 - \frac{3 * Senriched}{4 * Snormal}, \quad (1)$$

where $S_{enriched}$ and S_{normal} are the corresponding NMR signals for p-H_2 enriched and normal (i.e., non-enriched) hydrogen gas samples. Note the multipliers 3 and 4 are used to reflect the 75% o-H_2 in normal (unenriched) H_2 gas.[30] Three p-H_2 generators were tested for test-retest reproducibility.

Catalyst activation.

Catalyst activation was performed by heating the catalyst-containing spiral using a heat gun to >100 °C for ~15 minutes under continuous 150 sccm flow of H_2 gas.

^{13}C SABRE hyperpolarization of [1-^{13}C]pyruvate

^{13}C SABRE hyperpolarization of [1-^{13}C]pyruvate was performed using SABRE in SHield Enables Alignment Transfer to Heteronuclei (SABRE-SHEATH)[47–48] tailored for the ^{13}C nucleus[45, 76] using the DMSO-co-ligand approach developed by Duckett and co-workers.[74] Sodium [1-^{13}C]-pyruvate and deuterated methanol-d_4 solvent were purchased from Sigma-Aldrich and used without any further purification. The [IrCl(COD)(IMes)] SABRE catalyst precursor was synthesized according to a literature procedure.[21] The sample was prepared with a fixed ratio of substrate to Ir-IMes SABRE pre-catalyst and DMSO in 0.6 mL of methanol-d_4 in a 5 mm NMR tube with a typical ratio of substrate, catalyst (12 mM) and DMSO as 7:1:10. Ultra-high-purity H_2 gas (Airgas) was fed into a p-H_2 generator and enriched to about 50% para- fraction using liquid N_2 as described above. The p-H_2 flow is directed via PTFE tubing using MFC (Sierra Instruments SmartTrak 100 series) set at 80 sccm flow rate and directed to a conventional 5 mm NMR tube (Norell) to allow p-H_2 bubbling through the sample. The entire p-H_2 line was pressurized to 40 PSI overpressure. SABRE-SHEATH requires the use of micro- o sub-microtesla magnetic fields to enable efficient polarization transfer from p-H_2-derived hydrides to heteronucleus (*e.g.*, ^{13}C targeted here). In practice, these fields are achieved by attenuating the Earth's magnetic field, and creating a minute magnetic field inside the shield using electromagnet. Here, magnetic fields near or below ~1 μT were achieved with a home-built apparatus consisting of a solenoid coil placed inside a mu-metal shield (Magnetic Shield Corporation, model No. ZG-206). This solenoid is 41 mm in diameter: 40 mm core, 20 cm long windings with 220 turns AWG20 (0.9 mm) Cu wire and with 220 Ω resistor in series. The solenoid coil was

driven by commercial 1.5 V batteries with a variable-resistance decade box in series to provide finer control of the internal magnetic field of the shield, which is monitored using a Lakeshore Cryotronics Gaussmeter (Model No. 475 DSP with HMMA-2512-VR Hall Probe). NMR experiments were performed using a 1 T Magritek Spinsolve benchtop NMR spectrometer. All ^{13}C NMR spectra were taken without ^{1}H decoupling throughout the duration of the experiment. The time required to manually transfer the sample from the shield region to the magnet for low-field NMR acquisition was usually < 5 s. The ^{13}C signal enhancement was computed by comparing HP signal AUC to external ^{13}C signal thermal signal reference (4M sodium [1-^{13}C]acetate) using Eq. 2:

$$\varepsilon(^{13}C) = \frac{S_{HP}}{S_{REF}} \cdot \frac{C_{REF}}{C_{HP}} \cdot \frac{A_{REF}}{S_{HP}}, \quad (2)$$

where S_{HP} and S_{REF} are ^{13}C signals from HP [1-^{13}C]pyruvate and thermal signal reference [1-^{13}C]acetate, C_{REF} and C_{HP} are concentrations of thermal signal reference [1-^{13}C]acetate (4 M) and of HP [1-^{13}C]pyruvate, respectively, and A_{REF} and A_{HP} are effective cross-sections of the NMR tubes for the thermal signal reference [1-^{13}C]acetate and HP [1-^{13}C]pyruvate samples.

RESULTS AND DISCUSSION

Parahydrogen enrichment.

Three identical copies of the generator were employed for quality assurance prior to catalyst activation. Under conditions of liquid N_2 and 150 sccm p-H_2 flow rate, the bench-top NMR quantification yielded the following p-H_2 enrichment fractions: 48.4±0.5%, 48.1±0.5%, and 48.2±0.5% respectively, demonstrating the robustness of the design in the context of reproducible generator construction. A representative NMR quantification of p-H_2 fraction at 150 sccm flow rate is shown in Figure 3a. The remaining p-H_2 quantification studies were performed with one of the three devices. The flow rate was then varied from 150 sccm to 1000 sccm (Figure 3b, blue bars) clearly demonstrating the reduction of p-H_2 fraction with increased flow rate. This finding is rationalized as follows: the non-activated catalyst has some potency for ortho↔para conversion, which is sufficient for slow-flowing H_2 gas. When the flow rate is fast (*i.e.*, 1000 sccm), the slow ortho↔para conversion rate is no longer sufficient to allow the system to reach an equilibrium conversion while the gas moves along the catalyst-filled copper spiral, thus yielding a lower than expected p-H_2 fraction.

Catalyst activation by heating under H_2 atmosphere.

After catalyst activation in the copper spiral as described above, the performance of the same generator was evaluated at various flow rates (Figure 3b, red bars). The results clearly indicate that catalyst activation is indeed important in order to maximize the ortho↔para conversion, allowing the system to achieve full conversion at high flow rates up to 1,000 sccm. Although higher hydrogen flow rates were not tested due to limitations of the mass flow controller, we expect the generator to perform well at substantially higher flow rates of at least 4000 sccm. Our expectation is based on the performance of a recently published cryogenic design, which employs catalyst-filled copper tubing filled with half the quantity of

the catalyst (10 g vs. 21 g employed here) in smaller ID/OD copper tubing.[64] This recently published design performed well at flow rates of up to 4000 sccm.[64]

The utility of the parahydrogen generator for ^{13}C SABRE-SHEATH hyperpolarization.

Hyperpolarization of [1-^{13}C]pyruvate was evaluated using another copy of the generator at a different site. It was employed for SABRE hyperpolarization studies of [1-^{13}C]pyruvate using SABRE-SHEATH. The simultaneous exchange of p-H_2 and [1-^{13}C]pyruvate on activated Ir-IMes catalyst leads to buildup of ^{13}C hyperpolarization, Figure 4a. Figure 4b shows a representative spectrum of ^{13}C-hyperpolarized [1-^{13}C]-pyruvate with signal enhancement ε of over 14,000-fold, corresponding to P_{13C} of 1.2% obtained via comparison of the NMR signal intensity with a reference sample, Figure 4c.

If near-100% p-H_2 would have been employed, P_{13C} would be tripled to P_{13C} = 3.5%.[30] We note that P_{13C} strongly depends on the experimental conditions. To the best of our knowledge, the extrapolated P_{13C} value reported here exceeds the highest reported value (P_{13C} of ~1%)[74, 77] by more than threefold representing a substantial advancement for HP [1-^{13}C]pyruvate production via SABRE-SHEATH technique.

The pilot optimization of ^{13}C SABRE-SHEATH conditions reveal ^{13}C signal dependence on the microtesla magnetic field (Figure 5a), temperature (Figure 5b), polarization buildup time (*i.e.*, the duration of p-H_2 bubbling, Figure 5c) and catalyst concentration (Figure 5e). The ^{13}C T_1 in-shield relaxation value of 31±4 seconds at [catalyst]=7.8 mM are substantially longer than ^{15}N T_1 of ca. 12–15 s of [$^{15}N_3$]metronidazole at [catalyst]~2 mM[78] despite that fact that ^{13}C gyromagnetic ratio is 2.5 times greater than ^{15}N one and therefore ^{13}C spin would be more prone to the catalyst-induced relaxation. We rationalize this observation by greater distance of ^{13}C1 nucleus from Ir due to the presences of bridging oxygen (i.e., Ir-O=^{13}C) versus direct Ir interaction with ^{15}N nucleus (i.e., Ir-^{15}N). This observation is important because longer in-shield ^{13}C T_1 at microtesla magnetic field effectively results in greater P_{13C}.[78]

We envision that additional future additional improvements for ^{13}C pyruvate polarization can be made through increase of p-H_2 pressure and flow rate[79] and the use of recently reported hardware for more precise calibration of in-shield nanotelsa magnetic field.[80]

The reported results clearly demonstrate the utility of our generator to produce a HP state that can be easily detectable, even when using a bench-top NMR spectrometer operating at 1 T. We note that although ^{13}C1-labeled pyruvate was employed, the resonance at 205 ppm corresponds to natural ^{13}C abundance signal from ^{13}C2 locked in a singlet state with ^{13}C1.[77] Thus, we anticipate that our generator can enable a wide range of p-H_2 based hyperpolarization studies in the context of development, optimization and quality assurance of HP ^{13}C compounds and biocompatible contrast agents even at natural abundance ^{13}C level. We also anticipate that other nuclei (^{15}N, ^{19}F, ^{1}H, etc.) can also be readily studied using our low-cost and easy-to-maintain p-H_2 generator in combination with a bench-top NMR spectrometer. Such combination should provide a straightforward gateway to HP studies with p-H_2 for a wide range of laboratories.

CONCLUSIONS

In summary, we report a robust design of a p-H_2 generator developed for operation at liquid N_2 temperature based on many years of experience in our laboratories. We employed near real-time bench-top NMR spectroscopy for quantification of p-H_2 fraction, indicating p-H_2 enrichment of ~48% (3 separately constructed devices) at flow rates of up to 1000 sccm; moreover, it is expected that flow rates of up to 4000 sccm should be attainable without performance loss. Catalyst activation by heat under H_2 atmosphere was shown to be important for efficient operation at high flow rates. The utility of the generator has been investigated for SABRE-SHEATH ^{13}C-hyperpolarization of [1-^{13}C]pyruvate, the leading metabolic ^{13}C contrast agent under investigation in clinical trials. Despite low p-H_2 fraction resulting in ~3-fold signal reduction (vs. near-100% p-H_2), it was possible to successfully hyperpolarize [1-^{13}C]pyruvate for detection using a 1 T bench-top NMR spectrometer (ε~14,000, P_{13C}~1.2%). We anticipate that the reported generator design will be useful for those working on development of p-H_2-based hyperpolarization technologies (*e.g.*, PHIP and SABRE), and particularly those working on developing new biocompatible compounds that can be employed as exogenous HP contrast agents. Taken together, the combination of the described p-H_2 generator and a bench-top NMR spectrometer embodies a low-cost and robust gateway to the field to p-H_2 hyperpolarization without substantial investment in complex infrastructure. Although on-demand p-H_2 production for utility in SABRE hyperpolarization was demonstrated here, the produced p-H_2 gas can also be stored in an aluminum tank for weeks, because p-H_2 back conversion to normal hydrogen is slow.[36, 64]

ACKNOWLEDGMENT

Molecular Products Inc. for providing Ionex - Type O-P Catalyst. This work was supported by NSF CHE-1416268, CHE-1416432, CHE-1905341, and CHE-1904780, DOD CDMRP W81XWH-15-1-0271, W81XWH-15-1-0272, W81XWH-20-10576, and W81XWH-20-10578, NCI 1R21CA220137, NIBIB 1R01EB029829, and NHLBI 1R21HL154032. This project has been funded in whole or in part with federal funds from the National Cancer Institute, National Institutes of Health, under Contract No. HHSN261200800001E. B.M.G. acknowledges support from a Cottrell Scholar SEED Award from Research Corporation for Science Advancement. IVK and OGS acknowledge financial support from RFBR (19-29-10003) and the Russian Ministry of Science and Higher Education.

REFERENCES

1. Nikolaou P; Goodson BM; Chekmenev EY, NMR Hyperpolarization Techniques for Biomedicine. Chem. Eur. J 2015, 21 (8), 3156–3166. [PubMed: 25470566]
2. Goodson BM; Whiting N; Coffey AM; Nikolaou P; Shi F; Gust BM; Gemeinhardt ME; Shchepin RV; Skinner JG; Birchall JR; Barlow MJ; Chekmenev EY, Hyperpolarization Methods for MRS. Emagres 2015, 4 (4), 797–810.
3. Ardenkjaer-Larsen JH; Fridlund B; Gram A; Hansson G; Hansson L; Lerche MH; Servin R; Thaning M; Golman K, Increase in signal-to-noise ratio of > 10,000 times in liquid-state NMR. Proc. Natl. Acad. Sci. U. S. A 2003, 100 (18), 10158–10163. [PubMed: 12930897]
4. Ardenkjaer-Larsen JH, On the present and future of dissolution-DNP. J. Magn. Reson 2016, 264, 3–12. [PubMed: 26920825]
5. Golman K; Axelsson O; Johannesson H; Mansson S; Olofsson C; Petersson JS, Parahydrogen-induced polarization in imaging: Subsecond C-13 angiography. Magn. Reson. Med 2001, 46 (1), 1–5. [PubMed: 11443703]

6. Golman K; Ardenkjær-Larsen JH; Petersson JS; Månsson S; Leunbach I, Molecular imaging with endogenous substances. Proc. Natl. Acad. Sci. U. S. A 2003, 100 (18), 10435–10439. [PubMed: 12930896]
7. Golman K; in't Zandt R; Thaning M, Real-time metabolic imaging. Proc. Natl. Acad. Sci. U. S. A 2006, 103 (30), 11270–11275. [PubMed: 16837573]
8. Mugler JP; Altes TA, Hyperpolarized 129Xe MRI of the human lung. J. Magn. Reson. Imaging 2013, 37 (2), 313–331. [PubMed: 23355432]
9. Kovtunov KV; Pokochueva EV; Salnikov OG; Cousin S; Kurzbach D; Vuichoud B; Jannin S; Chekmenev EY; Goodson BM; Barskiy DA; Koptyug IV, Hyperpolarized NMR: d-DNP, PHIP, and SABRE. Chem. Asian J 2018, 13 (15), 1857–1871.
10. Rayner PJ; Duckett SB, Signal Amplification by Reversible Exchange (SABRE): From Discovery to Diagnosis. Angew. Chem. Int. Ed 2018, 57 (23), 6742–6753.
11. Brindle KM, Imaging Metabolism with Hyperpolarized ^{13}C-Labeled Cell Substrates. J. Am. Chem. Soc 2015, 137 (20), 6418–6427. [PubMed: 25950268]
12. Kurhanewicz J; Vigneron DB; Brindle K; Chekmenev EY; Comment A; Cunningham CH; DeBerardinis RJ; Green GG; Leach MO; Rajan SS; Rizi RR; Ross BD; Warren WS; Malloy CR, Analysis of Cancer Metabolism by Imaging Hyperpolarized Nuclei: Prospects for Translation to Clinical Research Neoplasia 2011, 13 (2), 81–97. [PubMed: 21403835]
13. Nelson SJ; Kurhanewicz J; Vigneron DB; Larson PEZ; Harzstark AL; Ferrone M; van Criekinge M; Chang JW; Bok R; Park I; Reed G; Carvajal L; Small EJ; Munster P; Weinberg VK; Ardenkjaer-Larsen JH; Chen AP; Hurd RE; Odegardstuen LI; Robb FJ; Tropp J; Murray JA, Metabolic Imaging of Patients with Prostate Cancer Using Hyperpolarized 1-C-13 Pyruvate. Sci. Transl. Med 2013, 5 (198), 198ra108.
14. Kurhanewicz J; Vigneron DB; Ardenkjaer-Larsen JH; Bankson JA; Brindle K; Cunningham CH; Gallagher FA; Keshari KR; Kjaer A; Laustsen C; Mankoff DA; Merritt ME; Nelson SJ; Pauly JM; Lee P; Ronen S; Tyler DJ; Rajan SS; Spielman DM; Wald L; Zhang X; Malloy CR; Rizi R, Hyperpolarized ^{13}C MRI: Path to Clinical Translation in Oncology. Neoplasia 2019, 21 (1), 1–16. [PubMed: 30472500]
15. Bowers CR; Weitekamp DP, Transformation of Symmetrization Order to Nuclear-Spin Magnetization by Chemical-Reaction and Nuclear-Magnetic-Resonance. Phys. Rev. Lett 1986, 57 (21), 2645–2648. [PubMed: 10033824]
16. Eisenschmid TC; Kirss RU; Deutsch PP; Hommeltoft SI; Eisenberg R; Bargon J; Lawler RG; Balch AL, Para Hydrogen Induced Polarization In Hydrogenation Reactions. J. Am. Chem. Soc 1987, 109 (26), 8089–8091.
17. Bowers CR; Weitekamp DP, Para-Hydrogen and Synthesis Allow Dramatically Enhanced Nuclear Alignment. J. Am. Chem. Soc 1987, 109 (18), 5541–5542.
18. Koptyug IV; Kovtunov KV; Burt SR; Anwar MS; Hilty C; Han SI; Pines A; Sagdeev RZ, Para-hydrogen-induced polarization in heterogeneous hydrogenation reactions. J. Am. Chem. Soc 2007, 129 (17), 5580–5586. [PubMed: 17408268]
19. Adams RW; Aguilar JA; Atkinson KD; Cowley MJ; Elliott PIP; Duckett SB; Green GGR; Khazal IG; Lopez-Serrano J; Williamson DC, Reversible Interactions with para-Hydrogen Enhance NMR Sensitivity by Polarization Transfer. Science 2009, 323 (5922), 1708–1711. [PubMed: 19325111]
20. Adams RW; Duckett SB; Green RA; Williamson DC; Green GGR, A theoretical basis for spontaneous polarization transfer in non-hydrogenative parahydrogen-induced polarization. J. Chem. Phys 2009, 131, 194505. [PubMed: 19929058]
21. Cowley MJ; Adams RW; Atkinson KD; Cockett MCR; Duckett SB; Green GGR; Lohman JAB; Kerssebaum R; Kilgour D; Mewis RE, Iridium N-Heterocyclic Carbene Complexes as Efficient Catalysts for Magnetization Transfer from para-Hydrogen. J. Am. Chem. Soc 2011, 133 (16), 6134–6137. [PubMed: 21469642]
22. Muhammad SR; Greer RB; Ramirez SB; Goodson BM; Fout AR, Cobalt-Catalyzed Hyperpolarization of Structurally Intact Olefins. ACS Catalysis 2021, 11 (4), 2011–2020.
23. Goldman M; Johannesson H; Axelsson O; Karlsson M, Hyperpolarization of C-13 through order transfer from parahydrogen: A new contrast agent for MFI. Magn. Reson. Imaging 2005, 23 (2), 153–157. [PubMed: 15833606]

24. Goldman M; Johannesson H; Axelsson O; Karlsson M, Design and implementation of C-13 hyperpolarization from para-hydrogen, for new MRI contrast agents. C. R. Chimie 2006, 9 (3–4), 357–363.
25. Bhattacharya P; Chekmenev EY; Perman WH; Harris KC; Lin AP; Norton VA; Tan CT; Ross BD; Weitekamp DP, Towards hyperpolarized ^{13}C-succinate imaging of brain cancer. J. Magn. Reson 2007, 186, 150–155. [PubMed: 17303454]
26. Hövener J-B; Chekmenev EY; Harris KC; Perman W; Robertson L; Ross BD; Bhattacharya P, PASADENA hyperpolarization of ^{13}C biomolecules: equipment design and installation. Magn. Reson. Mater. Phy 2009, 22, 111–121.
27. Bhattacharya P; Chekmenev EY; Reynolds WF; Wagner S; Zacharias N; Chan HR; Bünger R; Ross BD, Parahydrogen-induced polarization (PHIP) hyperpolarized MR receptor imaging in vivo: a pilot study of ^{13}C imaging of atheroma in mice. NMR Biomed 2011, 24 (8), 1023–1028. [PubMed: 21538638]
28. Perman WH; Bhattacharya P; Leupold J; Lin AP; Harris KC; Norton VA; Hoevener J-B; Ross BD, Fast volumetric spatial-spectral MR imaging of hyperpolarized (13)C-labeled compounds using multiple echo 3D bSSFP. Magn. Reson. Imaging 2011, 28 (4), 459–465.
29. Kadlecek S; Vahdat V; Nakayama T; Ng D; Emami K; Rizi R, A simple and low-cost device for generating hyperpolarized contrast agents using parahydrogen. NMR Biomed 2011, 24 (8), 933–942. [PubMed: 21845739]
30. Hövener J-B; Pravdivtsev AN; Kidd B; Bowers CR; Glöggler S; Kovtunov KV; Plaumann M; Katz-Brull R; Buckenmaier K; Jerschow A; Reineri F; Theis T; Shchepin RV; Wagner S; Bhattacharya P; Zacharias NM; Chekmenev EY, Parahydrogen-based Hyperpolarization for Biomedicine. Angew. Chem. Int. Ed 2018, 57 (35), 11140–11162.
31. Kovtunov KV; Koptyug IV; Fekete M; Duckett SB; Theis T; Joalland B; Chekmenev EY, Parahydrogen-induced Hyperpolarization of Gases. Angew. Chem. Int. Ed 2020, 59 (41), 17788–17797.
32. Green RA; Adams RW; Duckett SB; Mewis RE; Williamson DC; Green GGR, The theory and practice of hyperpolarization in magnetic resonance using parahydrogen. Prog. Nucl. Mag. Res. Spectrosc 2012, 67, 1–48.
33. Kovtunov KV; Zhivonitko VV; Skovpin IV; Barskiy DA; Koptyug IV, Parahydrogen-induced polarization in heterogeneous catalytic processes. Top. Curr. Chem 2013, 338, 123–180. [PubMed: 23097028]
34. Hövener J-B; Baer S; Leupold J; Jenne K; Leibfritz D; Hennig J; Duckett SB; von Elverfeldt D, A continuous-flow, high-throughput, high-pressure parahydrogen converter for hyperpolarization in a clinical setting. NMR Biomed 2013, 26 (2), 124–131. [PubMed: 22833391]
35. Tom BA; Bhasker S; Miyamoto Y; Momose T; McCall BJ, Producing and quantifying enriched para-H-2. Rev. Sci. Instrum 2009, 80 (1), 3.
36. Feng B; Coffey AM; Colon RD; Chekmenev EY; Waddell KW, A pulsed injection parahydrogen generator and techniques for quantifying enrichment. J. Magn. Reson 2012, 214, 258–262. [PubMed: 22188975]
37. Birchall JR; Coffey AM; Goodson BM; Chekmenev EY, High-Pressure Clinical-Scale 87% Parahydrogen Generator. Anal. Chem 2020, 92 (23), 15280–15284. [PubMed: 33170640]
38. Gamliel A; Allouche-Arnon H; Nalbandian R; Barzilay CM; Gomori JM; Katz-Brull R, An Apparatus for Production of Isotopically and Spin-Enriched Hydrogen for Induced Polarization Studies. Appl. Magn. Reson 2010, 39 (4), 329–345.
39. Farkas A, Orthohydrogen, Parahydrogen, and Heavy Hydrogen Cambridge University Press: Cambridge, 1935.
40. Bowers CR, Sensitivity Enhancement Utilizing Parahydrogen. In eMagRes, John Wiley & Sons, Ltd: 2007.
41. Goldman M; Johannesson H, Conversion of a proton pair para order into C-13 polarization by rf irradiation, for use in MRI. C. R. Physique 2005, 6 (4–5), 575–581.
42. Kadlecek S; Emami K; Ishii M; Rizi R, Optimal transfer of spin-order between a singlet nuclear pair and a heteronucleus. J. Magn. Reson 2010, 205 (1), 9–13. [PubMed: 20427216]

43. Baer S; Lange T; Leibfritz D; Hennig J; von Elverfeldt D; Hoevener J-B, On the spin order transfer from parahydrogen to another nucleus. J. Magn. Reson 2012, 225, 25–35. [PubMed: 23103392]
44. Cai C; Coffey AM; Shchepin RV; Chekmenev EY; Waddell KW, Efficient transformation of parahydrogen spin order into heteronuclear magnetization. J. Phys. Chem. B 2013, 117 (5), 1219–1224. [PubMed: 23214962]
45. Barskiy DA; Shchepin RV; Tanner CPN; Colell JFP; Goodson BM; Theis T; Warren WS; Chekmenev EY, The Absence of Quadrupolar Nuclei Facilitates Efficient 13C Hyperpolarization via Reversible Exchange with Parahydrogen. ChemPhysChem 2017, 18, 1493–1498. [PubMed: 28517362]
46. Bales L; Kovtunov KV; Barskiy DA; Shchepin RV; Coffey AM; Kovtunova LM; Bukhtiyarov AV; Feldman MA; Bukhtiyarov VI; Chekmenev EY; Koptyug IV; Goodson BM, Aqueous, Heterogeneous Parahydrogen-Induced 15N Polarization. J. Phys. Chem. C 2017, 121 (28), 15304–15309.
47. Theis T; Truong ML; Coffey AM; Shchepin RV; Waddell KW; Shi F; Goodson BM; Warren WS; Chekmenev EY, Microtesla SABRE Enables 10% Nitrogen-15 Nuclear Spin Polarization. J. Am. Chem. Soc 2015, 137 (4), 1404–1407. [PubMed: 25583142]
48. Truong ML; Theis T; Coffey AM; Shchepin RV; Waddell KW; Shi F; Goodson BM; Warren WS; Chekmenev EY, ^{15}N Hyperpolarization By Reversible Exchange Using SABRE-SHEATH. J. Phys. Chem. C 2015, 119 (16), 8786–8797.
49. Zhivonitko VV; Skovpin IV; Koptyug IV, Strong ^{31}P nuclear spin hyperpolarization produced via reversible chemical interaction with parahydrogen. Chem. Comm 2015, 51 (13), 2506–2509. [PubMed: 25358646]
50. Shchepin RV; Goodson BM; Theis T; Warren WS; Chekmenev EY, Toward Hyperpolarized ^{19}F Molecular Imaging via Reversible Exchange with Parahydrogen. ChemPhysChem 2017, 18 (15), 1961–1965. [PubMed: 28557156]
51. Plaumann M; Bommerich U; Trantzschel T; Lego D; Dillenberger S; Sauer G; Bargon J; Buntkowsky G; Bernarding J, Parahydrogen-Induced Polarization Transfer to ^{19}F in Perfluorocarbons for ^{19}F NMR Spectroscopy and MRI. Chem. Eur. J 2013, 19 (20), 6334–6339. [PubMed: 23526596]
52. Olaru AM; Burt A; Rayner PJ; Hart SJ; Whitwood AC; Green GGR; Duckett SB, Using signal amplification by reversible exchange (SABRE) to hyperpolarise Sn-119 and Si-29 NMR nuclei. Chem. Comm 2016, 52 (100), 14482–14485. [PubMed: 27904890]
53. Rayner PJ; Burns MJ; Olaru AM; Norcott P; Fekete M; Green GGR; Highton LAR; Mewis RE; Duckett SB, Delivering strong ^{1}H nuclear hyperpolarization levels and long magnetic lifetimes through signal amplification by reversible exchange. Proc. Natl. Acad. Sci. U. S. A 2017, 114 (16), E3188–E3194. [PubMed: 28377523]
54. Fekete M; Ahwal F; Duckett SB, Remarkable Levels of ^{15}N Polarization Delivered through SABRE into Unlabeled Pyridine, Pyrazine, or Metronidazole Enable Single Scan NMR Quantification at the mM Level. J. Phys. Chem. B 2020, 124 (22), 4573–4580. [PubMed: 32383603]
55. Korchak S; Mamone S; Glöggler S, Over 50% 1H and 13C Polarization for Generating Hyperpolarized Metabolites—A para-Hydrogen Approach. ChemistryOpen 2018, 7 (9), 672–676. [PubMed: 30191091]
56. Shchepin RV; Birchall JR; Chukanov NV; Kovtunov KV; Koptyug IV; Theis T; Warren WS; Gelovani JG; Goodson BM; Shokouhi S; Rosen MS; Yen Y-F; Pham W; Chekmenev EY, Hyperpolarizing Concentrated Metronidazole $^{15}NO_2$ Group Over Six Chemical Bonds with More Than 15% Polarization and 20 Minute Lifetime. Chem. Eur. J 2019, 25, 8829–8836. [PubMed: 30964568]
57. Reineri F; Boi T; Aime S, ParaHydrogen Induced Polarization of ^{13}C carboxylate resonance in acetate and pyruvate. Nat. Commun 2015, 6, 5858. [PubMed: 25556844]
58. Hövener J-B; Chekmenev EY; Harris KC; Perman W; Tran T; Ross BD; Bhattacharya P, Quality assurance of PASADENA hyperpolarization for ^{13}C biomolecules. Magn. Reson. Mater. Phy 2009, 22, 123–134.

59. Bhattacharya P; Harris K; Lin AP; Mansson M; Norton VA; Perman WH; Weitekamp DP; Ross BD, Ultra-fast three dimensional imaging of hyperpolarized C-13 in vivo. Magn. Reson. Mater. Phy 2005, 18 (5), 245–256.
60. Tam S; Fajardo ME, Ortho/para hydrogen converter for rapid deposition matrix isolation spectroscopy. Rev. Sci. Instrum 1999, 70 (4), 1926–1932.
61. Knopp G; Kirch K; Beaud P; Mishima K; Spitzer H; Radi P; Tulej M; Gerber T, Determination of the ortho-/para deuterium concentration ratio with femtosecond CARS. Journal of Raman Spectroscopy 2003, 34 (12), 989–993.
62. Parrott AJ; Dallin P; Andrews J; Richardson PM; Semenova O; Halse ME; Duckett SB; Nordon A, Quantitative In Situ Monitoring of Parahydrogen Fraction Using Raman Spectroscopy. Applied Spectroscopy 2019, 73 (1), 88–97. [PubMed: 30203662]
63. Du Y; Zhou R; Ferrer M-J; Chen M; Graham J; Malphurs B; Labbe G; Huang W; Bowers CR, An inexpensive apparatus for up to 97% continuous-flow parahydrogen enrichment using liquid helium. J. Magn. Reson 2020, 321, 106869. [PubMed: 33197680]
64. Nantogma S; Joalland B; Wilkens K; Chekmenev EY, Clinical-Scale Production of Nearly Pure (>98.5%) Parahydrogen and Quantification by Benchtop NMR Spectroscopy. Anal. Chem 2021, 93 (7), 3594–3601. [PubMed: 33539068]
65. Semenova O; Richardson PM; Parrott AJ; Nordon A; Halse ME; Duckett SB, Reaction Monitoring Using SABRE-Hyperpolarized Benchtop (1 T) NMR Spectroscopy. Anal. Chem 2019, 91 (10), 6695–6701. [PubMed: 30985110]
66. Joalland B; Schmidt A; Kabir MSH; Chukanov NV; Kovtunov KV; Koptyug IV; Hennig J; Hövener J-B; Chekmenev EY, Pulse-Programmable Magnetic Field Sweeping of Parahydrogen-Induced Polarization by Side Arm Hydrogenation. Anal. Chem 2020, 92, 1340–1345. [PubMed: 31800220]
67. Chae H; Min S; Jeong HJ; Namgoong SK; Oh S; Kim K; Jeong K, Organic Reaction Monitoring of a Glycine Derivative Using Signal Amplification by Reversible Exchange-Hyperpolarized Benchtop Nuclear Magnetic Resonance Spectroscopy. Anal. Chem 2020, 92 (16), 10902–10907. [PubMed: 32567842]
68. Zacharias NM; McCullough CR; Wagner S; Sailasuta N; Chan HR; Lee Y; Hu J; Perman WH; Henneberg C; Ross BD; Bhattacharya P, Towards Real-time Metabolic Profiling of Cancer with Hyperpolarized Succinate. J. Mol. Imaging Dyn 2016, 6 (1), 123. [PubMed: 27547490]
69. Shchepin RV; Barskiy DA; Coffey AM; Manzanera Esteve IV; Chekmenev EY,, Efficient Synthesis of Molecular Precursors for Para-Hydrogen-Induced Polarization of Ethyl Acetate-1-^{13}C and Beyond. Angew. Chem. Int. Ed 2016, 55 (20), 6071–6074.
70. Reineri F; Viale A; Giovenzana G; Santelia D; Dastru W; Gobetto R; Aime S, New Hyperpolarized Contrast Agents for C-13-MRI from Para-Hydrogenation of Oligooxyethylenic Alkynes. J. Am. Chem. Soc 2008, 130 (45), 15047–15053. [PubMed: 18922000]
71. Reineri F; Viale A; Dastrù W; Gobetto R; Aime S, How to design 13C para-hydrogen-induced polarization experiments for MRI applications. Contrast Media Mol. Imaging 2011, 6 (2), 77–84. [PubMed: 21504062]
72. Emmett PH; Harkness RW, The Catalytic Interconversion of Ortho—Para Hydrogen over Iron, Platinum and Nickel Catalysts. J. Am. Chem. Soc 1935, 57 (9), 1624–1631.
73. Das T; Kweon S-C; Nah IW; Karng SW; Choi J-G; Oh I-H, Spin conversion of hydrogen using supported iron catalysts at cryogenic temperature. Cryogenics 2015, 69 (Supplement C), 36–43.
74. Iali W; Roy SS; Tickner BJ; Ahwal F; Kennerley AJ; Duckett SB, Hyperpolarising Pyruvate through Signal Amplification by Reversible Exchange (SABRE). Angew. Chem. Int. Ed 2019, 58 (30), 10271–10275.
75. Merritt M; Harrison C; Storey C; Jeffrey F; Sherry A; Malloy C, Hyperpolarized C-13 allows a direct measure of flux through a single enzyme-catalyzed step by NMR. Proc. Natl. Acad. Sci. U. S. A 2007, 104 (50), 19773–19777. [PubMed: 18056642]
76. Gemeinhardt ME; Limbach MN; Gebhardt TR; Eriksson CW; Eriksson SL; Lindale JR; Goodson EA; Warren WS; Chekmenev EY; Goodson BM, "Direct" ^{13}C Hyperpolarization of ^{13}C-Acetate by MicroTesla NMR Signal Amplification by Reversible Exchange (SABRE). Angew. Chem. Int. Ed 2020, 59 (1), 418–423.

77. Tickner BJ; Semenova O; Iali W; Rayner PJ; Whitwood AC; Duckett SB, Optimisation of pyruvate hyperpolarisation using SABRE by tuning the active magnetisation transfer catalyst. Catal. Sci. Tech 2020, 10 (5), 1343–1355.

78. Birchall JR; Kabir MSH; Salnikov OG; Chukanov NV; Svyatova A; Kovtunov KV; Koptyug IV; Gelovani JG; Goodson BM; Pham W; Chekmenev EY, Quantifying the effects of quadrupolar sinks via ^{15}N relaxation dynamics in metronidazoles hyperpolarized via SABRE-SHEATH. Chem. Comm 2020, 56 (64), 9098–9101. [PubMed: 32661534]

79. Salnikov OG; Chukanov NV; Svyatova A; Trofimov IA; Kabir MSH; Gelovani JG; Kovtunov KV; Koptyug IV; Chekmenev EY, ^{15}N NMR Hyperpolarization of Radiosensitizing Antibiotic Nimorazole via Reversible Parahydrogen Exchange in Microtesla Magnetic Fields. Angew. Chem. Int. Ed 2021, 60 (5), 2406–2413.

80. Joalland B; Nantogma S; Chowdhury MRH; Nikolaou P; Chekmenev EY, Magnetic Shielding of Parahydrogen Hyperpolarization Experiments for the Masses. Magn. Reson. Chem 2021, doi: 10.1002/mrc.5167.

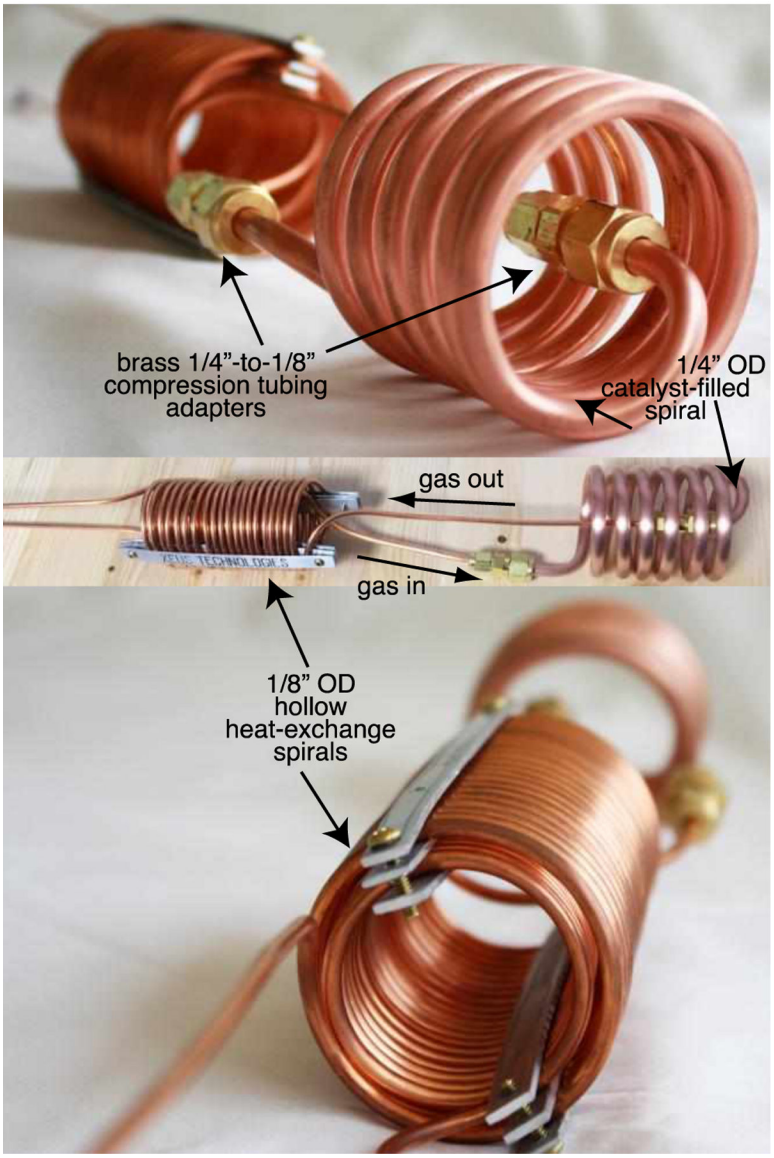

Figure 1.
Photographs of the p-H_2 generator device core, outlining the orientations and interfaces of key components.

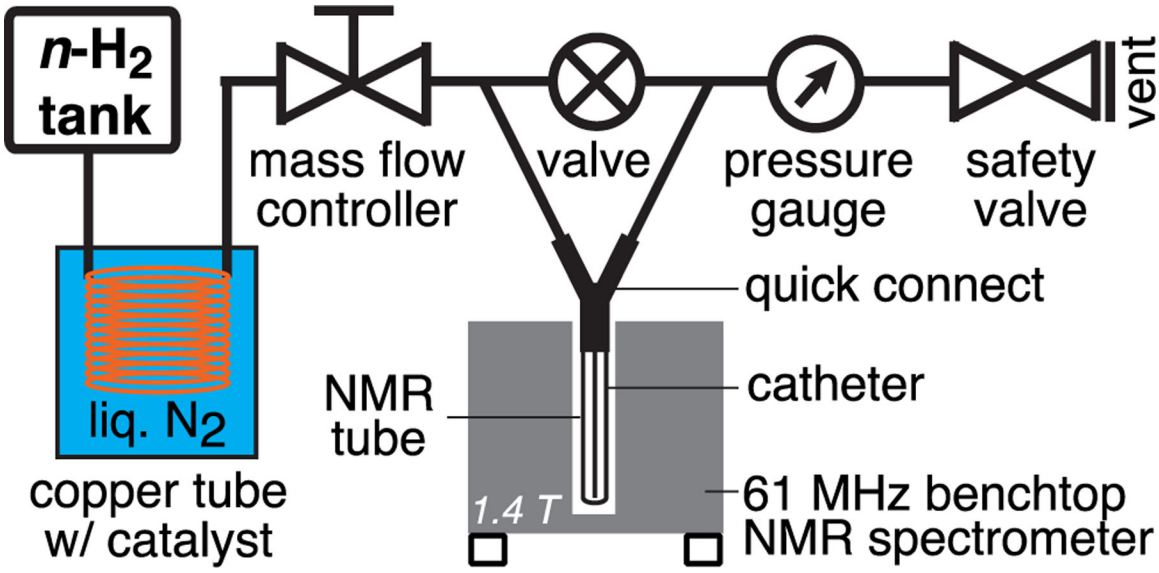

Figure 2.

Experimental setup schematic employed for p-H_2 quantification studies using real-time bench-top 1.4 T NMR spectroscopy. The safety valve allows for 100 PSI overpressure, and the normal hydrogen (n-H_2) pressure of the main hydrogen tank was set to 125 PSI. Switching the valve to the “OFF” position directs hydrogen gas to an NMR tube via a 0.065 in. OD Teflon catheter.

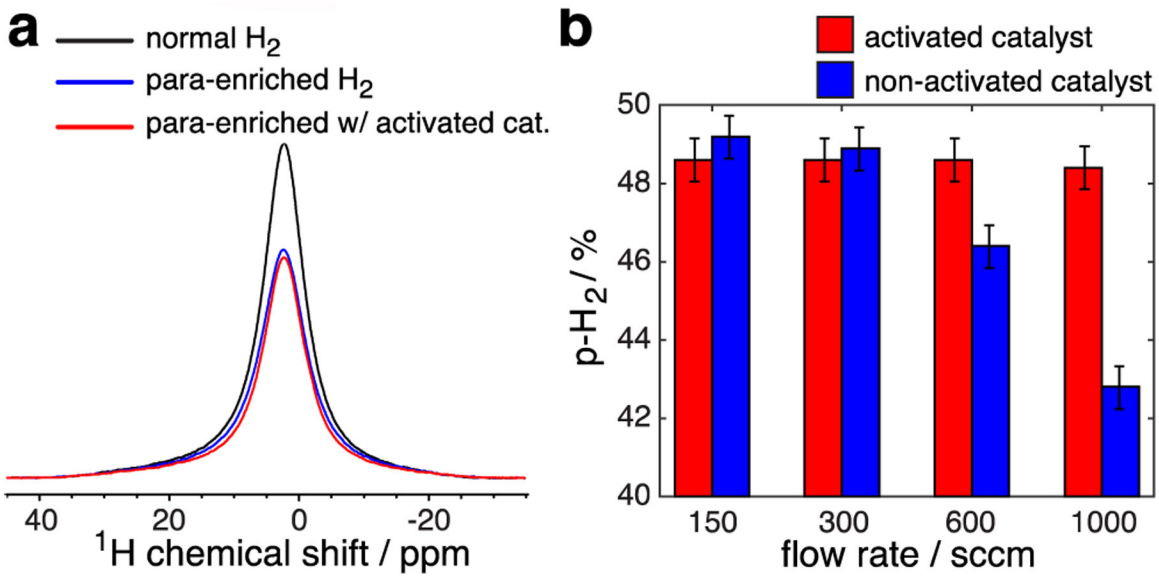

Figure 3.

a) Parahydrogen quantification using a 1.4 T NMR spectrometer operating at 61 MHz proton resonance frequency using gas samples at 8 atm (100 PSI overpressure). Acquisition parameters: 1024 scans, 5 kHz spectral width, 52 ms acquisition time, 0.1 s repetition time, ~102 s total acquisition time, 90° excitation pulse (~10 μs long). b) Dependence of p-H_2 fraction on the flow rate for activated and non-activated catalyst.

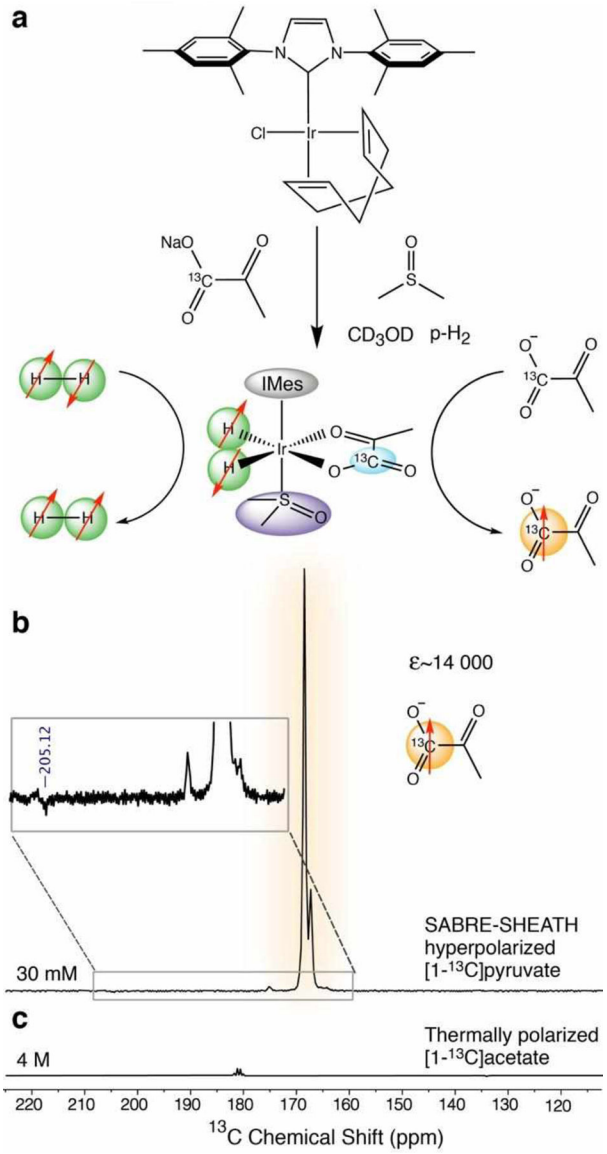

Figure 4.

a) Schematic of the catalytic system for SABRE-SHEATH hyperpolarization. Activated Ir complex catalyst, [Ir(H_2)(η^2-pyruvate)(DMSO)(IMes)], transfers magnetization from p-H_2 to [1-^{13}C]pyruvate through a J-coupled spin network. Both p-H_2 and pyruvate have weak, transient binding to the iridium complex. b) Single-scan HP ^{13}C spectrum selected from SABRE-SHEATH experiments; enhancement ε~14,000. Sample: 30 mM sodium [1-^{13}C]pyruvate, 20 mM DMSO, 7.8 mM Ir-IMes catalyst in methanol-d_4; spectrum acquired immediately following manual sample transfer to 1 T after 55 s p-H_2 bubbling at B_T=−0.7 μT. The inset of (b) shows a close-up ^{13}C spectrum. c) Single-scan thermally polarized ^{13}C signal from 4 M sodium [1-^{13}C]acetate using similar acquisition parameters.

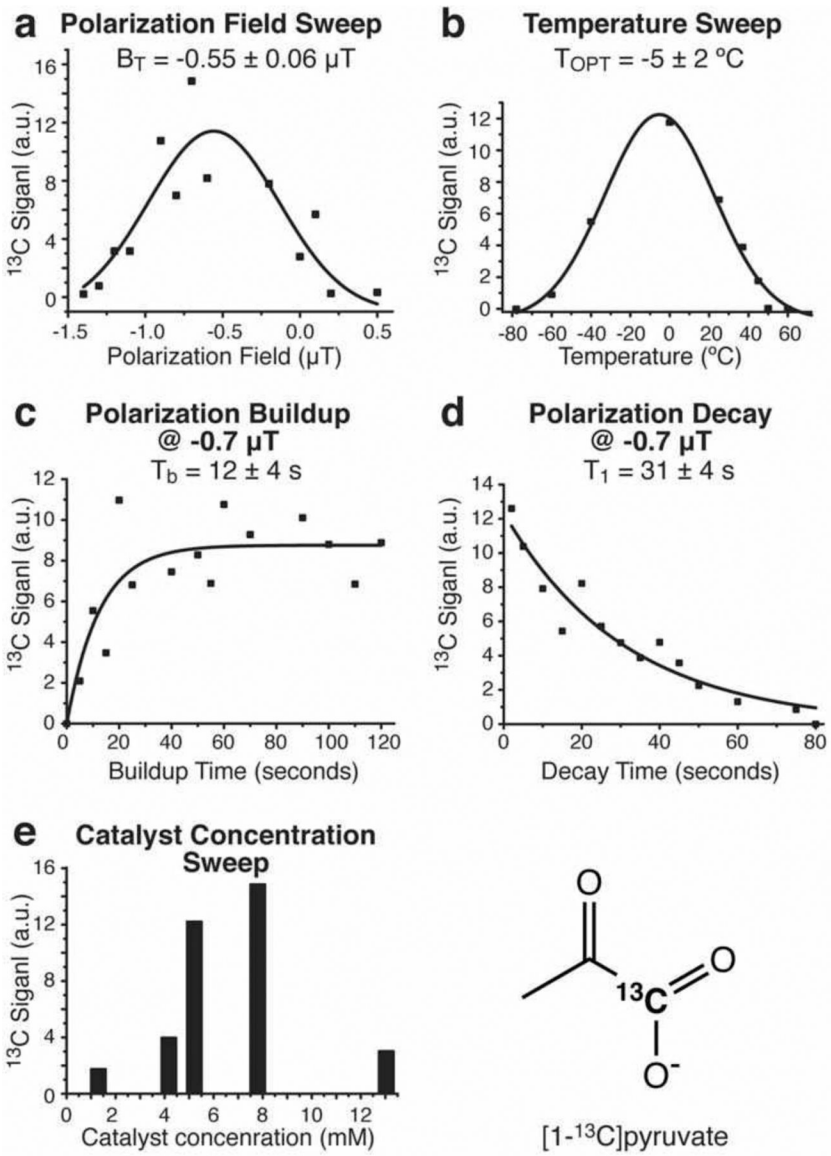

Figure 5.

Pilot optimization of SABRE-SHEATH hyperpolarization of [1-^{13}C]pyruvate: a) magnetic field sweep of a sample of [Ir(COD)(IMes)] (13 mM) with sodium [1-^{13}C]pyruvate (90 mM) and DMSO (120 mM) in 0.6 mL methanol-d_4 at room temperature; b) temperature sweep of a sample of [Ir(COD)(IMes)] (7.8 mM) sodium [1-^{13}C]pyruvate (30 mM) and DMSO (20 mM) in 0.6 mL methanol-d_4 at B_T=−0.7 μT; c) p-H_2 bubbling duration sweep using a sample of [Ir(COD)(IMes)] (7.8 mM) with sodium [1-^{13}C]pyruvate (30 mM) and DMSO (20 mM) in 0.6 mL methanol-d_4 at B_T=−0.7 μT; d) In-shield ^{13}C T_1 signal decay using a sample of [Ir(COD)(IMes)] (7.8 mM) with sodium [1-^{13}C]pyruvate (30 mM) and DMSO (20 mM) in 0.6 mL methanol-d_4 at B_T=−0.7 μT; e) SABRE catalyst concentration sweep using samples of 30 mM of sodium [1-^{13}C]pyruvate and 20 mM DMSO in 0.6 mL methanol-d_4 at B_T=−0.7 μT. All experiments were performed using with 100 PSI p-H_2 (~50% *para*-) overpressure at ~100 sccm flow rate.